Density-functional theory and Monte Carlo simulations of the phase behavior of a simple model liquid crystal

Stefano Giura[1] and Martin Schoen[1,2,*]

[1]*Stranski-Laboratorium für Physikalische und Theoretische Chemie, Fakultät für Mathematik und Naturwissenschaften, Technische Universität Berlin, Straße des 17. Juni 115, 10623 Berlin, Germany*

[2]*Department of Chemical and Biomolecular Engineering, Engineering Building I, Box 7905, North Carolina State University, 911 Partners Way, Raleigh, North Carolina 27695, USA*

(Received 13 May 2014; revised manuscript received 11 August 2014; published 29 August 2014)

We consider the phase behavior of a simple model of a liquid crystal by means of modified mean-field density-functional theory (MMF DFT) and Monte Carlo simulations in the grand canonical ensemble (GCEMC). The pairwise additive interactions between liquid-crystal molecules are modeled via a Lennard-Jones potential in which the attractive contribution depends on the orientation of the molecules. We derive the form of this orientation dependence through an expansion in terms of rotational invariants. Our MMF DFT predicts two topologically different phase diagrams. At weak to intermediate coupling of the orientation dependent attraction, there is a discontinuous isotropic-nematic liquid-liquid phase transition in addition to the gas-isotropic liquid one. In the limit of strong coupling, the gas-isotropic liquid critical point is suppressed in favor of a fluid-(gas- or isotropic-) nematic phase transition which is always discontinuous. By considering three representative isotherms in parallel GCEMC simulations, we confirm the general topology of the phase diagram predicted by MMF DFT at intermediate coupling strength. From the combined MMF DFT-GCEMC approach, we conclude that the isotropic-nematic phase transition is very weakly first order, thus confirming earlier computer simulation results for the same model [see M. Greschek and M. Schoen, Phys. Rev. E **83**, 011704 (2011)].

DOI: 10.1103/PhysRevE.90.022507 PACS number(s): 61.30.−v, 05.20.Jj, 64.60.A−, 64.60.fd

I. INTRODUCTION

Liquid crystals are an interesting class of soft-matter materials with a broad spectrum of applications. These range from the more traditional ones in display technology [1,2] over biosensors [3–5] and tribological applications [6] to photonic [7,8] and organic electronic devices [9,10]. Even in the food industry, liquid crystals are used to stabilize dispersions and emulsions [11].

In view of the diversity of applications for liquid-crystalline materials, a deeper theoretical understanding of their properties is a necessary prerequisite. As a first step in such a venture, the nature of various phase transitions in liquid crystals needs to be elucidated. In the context of this work, the isotropic-nematic (IN) phase transition is of particular relevance.

Theoretically, this phase transition has been studied by purely phenomenological approaches such as Landau theory which is an expansion of the free energy in terms of the alignment tensor where one retains terms that are necessary to describe a first-order phase transition [12]. In 1949, Onsager proposed a theory that allows one to understand the IN phase transition in a fluid of hard rods [13]. He could show that the Helmholtz energy of such a system can be decomposed into an energylike contribution and another one accounting for the entropy of mixing in a multicomponent mixture composed of rods with different orientations. Later, Maier and Saupe developed a mean-field theory of the IN phase transition where they assume an interaction contribution to the Gibbs energy depending quadratically on the nematic order parameter. The total Gibbs energy is then minimized with respect to the orientation distribution function [14–16].

Due to the steady and enormous increase in computer power since about the middle of the last century, computer-based theoretical approaches have gained a lot of insight into details of the IN phase transition in various model systems. For example, Eppenga and Frenkel studied the IN phase transition in a system composed of hard platelets [17]. Another shape of liquid-crystal molecules (i.e., mesogens) that has frequently been considered is that of a spherocylinder. If the interaction between a pair of spherocylinders is "hard" (i.e., infinitely repulsive with vanishing range), McGrother *et al.* determined the phase diagram by means of Monte Carlo (MC) computer simulations in the isothermal-isobaric ensemble [18].

Jungblut *et al.* studied a binary mixture of hard spherocylinders and hard spheres both in the bulk and in confinement [19]. Because of the presence of the spherical particles (representing a polymeric compound), a depletion attraction exists in this model very much akin to that in the Asakura-Oosawa-Vrij model [20,21]. By using a combination of a free-volume theory developed by Lekkerkerker and Stroobants [22] and grand canonical ensemble MC (GCEMC) simulations, Jungblut *et al.* investigate the phase behavior of their model which exhibits an IN phase transition in the bulk (see also Sec. VI).

Another interesting model has been proposed by Kihara [23]. Here, the interaction between a pair of spherocylinders has soft repulsive and attractive contributions. The phase diagram of the Kihara model liquid crystal has been examined by Cuetos *et al.* in detail [24].

Perhaps the most widely used potential in the study of the phase behavior of liquid crystals is the Gay-Berne model [25] which may be viewed as an improved overlap-potential model suggested earlier by Berne and Pechukas [26]. The phase diagram of the Gay-Berne liquid crystal has been determined by de Miguel *et al.* [27]. The clear advantage of the Gay-Berne model, on the one hand, is that it is a single interaction site

*Corresponding author: martin.schoen@tu-berlin.de

potential for elongated molecules. One clear disadvantage of the model, on the other hand, is that the potential parameters have a rather complicated orientation dependence which makes the Gay-Berne potential computationally quite costly.

For this study, we therefore decided to employ a rather simple potential model that is computationally inexpensive. In this so-called Hess-Su model [28], the distance dependence of the interactions at fixed mesogenic orientation is described by a Lennard-Jones potential. The orientation dependence is accounted for by an anisotropy function constructed such that the symmetry of the interaction between slightly elongated mesogens is represented correctly. Because the mesogens have an aspect ratio only slightly larger than one, GCEMC simulations are relatively easy. However, for higher densities, a problem may arise due to the inevitable deletion and creation of molecules during the course of a GCEMC simulation [29]. These two processes quickly become prohibitively inefficient at liquidlike densities.

The motivation to conduct this study is the following. From a finite-size scaling study of the IN phase transition, Greschek and Schoen could demonstrate that in the Hess-Su model the intersection of second-order cumulants of moments of the order-parameter distribution is independent of system size [30]. This is what one would expect for a continuous phase transition. At the same time, Greschek and Schoen showed that the correlation length at the IN transition is of the order of a few molecular diameters which would be indicative of a first-order transition. If the transition were indeed weakly first order, both a discontinuous change in density at the IN phase transitions should be minute and the change of the order parameter around the transition should be smeared out. In order to shed more light on the phase behavior, it is therefore desirable to consider the whole phase diagram and its topology. Because this would be a demanding task using MC simulations, we employ density-functional theory (DFT) complemented by GCEMC simulations for a few most interesting thermodynamic states.

The remainder of this work is organized as follows. In Sec. II, we introduce the Hess-Su model and focus in particular on deriving the anisotropy function describing the orientation dependence of the interaction between a pair of mesogens. Section III summarizes some key concepts of the modified mean-field (MMF) DFT approach adopted here. In Sec. IV, we give a similar account of the GCEMC method and quantities of interest to be computed. Our results are presented in Sec. V and summarized and discussed in the concluding Sec. VI.

II. MODEL

We consider N mesogens with pairwise additive intermolecular interactions such that the total configurational energy may be cast as

$$U(\boldsymbol{R},\boldsymbol{\Omega}) = \frac{1}{2}\sum_{i=1}^{N}\sum_{\substack{j=1\\ j\neq i}}^{N}\varphi(\boldsymbol{r}_{ij},\omega_i,\omega_j). \tag{2.1}$$

In Eq. (2.1), $\boldsymbol{r}_{ij} = \boldsymbol{r}_i - \boldsymbol{r}_j$ denotes the distance vector between the centers of mass of mesogens i and j located at $\boldsymbol{r}_i$ and $\boldsymbol{r}_j$, respectively. We also introduce shorthand notations for the set of center-of-mass positions $\boldsymbol{R} \equiv \{\boldsymbol{r}_1,\boldsymbol{r}_1,\ldots,\boldsymbol{r}_N\}$ and the set of polar angles $\boldsymbol{\Omega} \equiv \{\omega_i,\omega_j,\ldots,\omega_N\}$ specifying the orientations of the mesogens. Here, $\omega_i \equiv (\theta_i,\phi_i)$ assuming the mesogens to have uniaxial symmetry where θ_i and ϕ_i are Euler angles.

To proceed, we assume that $\varphi(\boldsymbol{r}_{ij},\omega_i,\omega_j)$ can be decomposed into an isotropic and an anisotropic part according to (see Chap. 2.2 of Ref. [31])

$$\varphi(\boldsymbol{r}_{ij},\omega_i,\omega_j) = \varphi_{\rm iso}(r_{ij}) + \varphi_{\rm anis}(\boldsymbol{r}_{ij},\omega_i,\omega_j), \tag{2.2}$$

where $r_{ij} = |\boldsymbol{r}_{ij}|$. We take the standard Lennard-Jones potential for the isotropic part, that is,

$$\begin{aligned}\varphi_{\rm iso}(r_{ij}) &= 4\varepsilon\left[\left(\frac{\sigma}{r_{ij}}\right)^{12} - \left(\frac{\sigma}{r_{ij}}\right)^{6}\right]\\ &\equiv \varphi_{\rm rep}(r_{ij}) + \varphi_{\rm att}(r_{ij}),\end{aligned} \tag{2.3}$$

where ε is the depth of the attractive well and σ is the "diameter" of a spherically symmetric reference molecule.

A. Expansion in rotational invariants

To obtain a closed expression for $\varphi_{\rm anis}$ we notice that for linear molecules, we can generally expand this quantity according to (see Chap. 2.3 of Ref. [31])

$$\varphi_{\rm anis}(\boldsymbol{r}_{ij},\omega_i,\omega_j) = \sum_{l_i l_j l}\varphi_{l_i l_j l}(r_{ij})\Phi_{l_i l_j l}(\omega_i,\omega_j,\omega), \tag{2.4}$$

where l_i ($i = 1,2$) and l are positive, semidefinite integers, $\varphi_{l_i l_j l}$ is an expansion coefficient that depends only on the distance $r_{ij} = |\boldsymbol{r}_{ij}|$, and

$$\begin{aligned}\Phi_{l_i l_j l}(\omega_i,\omega_j,\omega) \equiv \sum_{m_i m_j m} & C(l_i l_j l; m_i m_j m)\\ & \times \mathcal{Y}_{l_i m_i}(\omega_i)\mathcal{Y}_{l_j m_j}(\omega_j)\mathcal{Y}^{*}_{lm}(\omega)\end{aligned} \tag{2.5}$$

is a so-called rotational invariant. In Eq. (2.5), C denotes a Clebsch-Gordan coefficient, $\mathcal{Y}$ is a spherical harmonic, and the asterisk denotes the complex conjugate. The solid angle ω describes the orientation of $\hat{\boldsymbol{r}}_{ij} \equiv \boldsymbol{r}_{ij}/r_{ij}$ in a space-fixed frame of reference. Throughout this work, the caret is used to indicate a unit vector. The integer $m_i \in \{-l_i,\ldots,l_i\}$ where a similar relation holds also for the pairs (l_j,m_j) and (l,m).

Because the spherical harmonics form a complete orthonormal set of functions [see, for example, Eq. (A.39) of Ref. [31]], the rotational invariants form a complete set of functions as well. However, only a subset of rotational invariants needs to be considered here on account of symmetry considerations. As explained in Chap. 2.3 of Ref. [31], the interaction potential between a pair of linear molecules must be invariant if molecules i and j interchange their identity. This corresponds to a transformation in which ω_i, ω_j, and ω are replaced by new variables $\omega_i' = \omega_j$, $\omega_j' = \omega_i$, and $\omega' = -\omega$. Because of the parity relation for spherical harmonics [see also Eq. (A.47) of Ref. [31]]

$$\mathcal{Y}_{lm}(-\omega) = (-1)^l\mathcal{Y}_{lm}(\omega), \tag{2.6}$$

$\varphi_{\rm anis}$ in Eq. (2.4) remains unaltered upon interchanging mesogens i and j only if l is restricted to even integers or zero in the expansion (2.5).

In addition, one assumes the mesogens to possess head-tail symmetry (which is the case for quite a few organic molecules exhibiting liquid-crystalline properties; see, for example, pp. 3–10 of Ref. [12]). The term "head-tail symmetry" refers to the fact that φ_{anis} should also be invariant if one inverts the orientation of *either* mesogen i *or* mesogen j [i.e., by replacing in Eqs. (2.4) and (2.5) ω_i by $\omega_i' = -\omega_i$ *or* $\omega_j' = -\omega_j$ while maintaining the sign of *either* ω_j *or* ω_i, respectively]. The parity relation (2.6) then implies that either l_i or l_j must be even as well or equal to zero. Because our mesogens are identical, the label (i or j) they carry is meaningless from a physics point of view. This implies that the symmetry properties of the interaction potential can only be preserved if *both* l_i and l_j are restricted to even integers or vanish independently.

B. Selection rules for Clebsch-Gordan coefficients

Next, one uses the fact that only some of the Clebsch-Gordan coefficients in Eq. (2.5) are nonzero. For example, nonvanishing Clebsch-Gordan coefficients must satisfy the triangle inequality

$$|l_i - l_j| \leqslant l \leqslant l_i + l_j \tag{2.7}$$

[see Eq. (A.131) of Ref. [31]]. However, even though this selection rule limits the number of terms to be considered in the triple sum in Eq. (2.4) to some extent, an increasingly larger number of terms has to be considered the larger l_i, l_j, and l become. This number of terms becomes overwhelming rather quickly. Therefore, the triple sum in Eq. (2.4) needs to be truncated at some point if the approach outlined here is to be of any practical use.

In the following, we will therefore restrict the discussion to $l_{i,j} \leqslant 2$. Because of Eq. (2.7), one needs to consider in Eq. (2.4) only contributions involving the six rotational invariants Φ_{000}, Φ_{022}, Φ_{202}, Φ_{220}, Φ_{222}, and Φ_{224}.

These rotational invariants can be subsumed into three groups according to the following criteria. The first group consists of Φ_{000} as its only member. Because of $l_i = l_j = l = 0$ we also have $m_i = m_j = m = 0$. Therefore, the triple sum in Eq. (2.5) vanishes altogether such that $\Phi_{000} = (4\pi)^{-3/2}$ because $C(000;000) = 1$ and because of the definition of $\mathcal{Y}_{00} = (4\pi)^{-1/2}$.

The second group is composed of three rotational invariants which have in common that one of the indices $\{l_i, l_j, l\}$ is zero whereas the remaining two are equal. To find out which terms survive in Eq. (2.5), one needs to employ the relation

$$m = m_i + m_j \tag{2.8}$$

which establishes a second selection rule (besides the triangle inequality) for nonzero Clebsch-Gordan coefficients. These nonvanishing coefficients obtain for the set $\{l_i, l_j, l, m_i, m_j, m\}$ only if both selection rules are satisfied simultaneously [see also Eqs. (A.130) and (A.131) of Ref. [31]]. Therefore, the triple sum in Eq. (2.5) reduces to a single one.

The third group contains two members, namely, Φ_{222} and Φ_{224}. These two rotational invariants share as their common characteristic that none of the indices $\{l_i, l_j, l\}$ vanish. Hence, because of the second selection rule the triple sum in Eq. (2.5) remains. As a consequence, a much larger number of orientation dependent terms survive. To limit the calculational burden we assume that the refinement of φ_{anis} accomplished by incorporating terms proportional to Φ_{222} and Φ_{224} in Eq. (2.4) is negligibly small. Therefore, these terms will be ignored henceforth in the approximate representation of φ_{anis}.

To obtain a closed expression for φ_{anis}, the expansion coefficients $\varphi_{l_i l_j l}$ in Eq. (2.4) need to be determined. Because our mesogens are uncharged and nonpolar we focus exclusively on dispersion interactions. One can then show (see Chap. 2.6 of Ref. [31]) that $\varphi_{l_i l_j l} \propto r_{ij}^{-6}$ irrespective of the integers l_i, l_j, and l. In particular, $\varphi_{000} = \varphi_{\text{att}}$ where ε [see Eq. (2.3)] depends on the static polarizabilities along the principal axes of the linear mesogens. In a similar fashion, the constants of proportionality for the other expansion coefficients depend on a couple of numerical constants and various combinations of the static polarizability that we combine into two dimensionless constants ε_1 and ε_2, such that $\varepsilon_1\varepsilon$ and $\varepsilon_2\varepsilon$ account for the strengths of interaction associated with these different polarizabilities. However, the precise dependence of both constants on the static polarizabilities is of no concern in this work. Instead, we refer the interested reader to Chap. 2.6 of the book by Gray and Gubbins [31]. Thus, we obtain

$$\varphi_{\text{anis}}(\boldsymbol{r}_{ij}, \omega_i, \omega_j) = \varphi_{\text{att}}(r_{ij}) \Psi(\widehat{\boldsymbol{r}}_{ij}, \omega_i, \omega_j), \tag{2.9}$$

where the anisotropy function may be cast as

$$\frac{\Psi(\widehat{\boldsymbol{r}}_{ij}, \omega_i, \omega_j)}{(4\pi)^{3/2}\sqrt{5}} = \varepsilon_1 \Phi_{220} + \frac{\sqrt{5}\,\varepsilon_2}{5}(\Phi_{202} + \Phi_{022}) \tag{2.10}$$

and we dropped the arguments of the rotational invariants for notational convenience.

For the computer simulations to be presented and discussed below a slightly different form of Ψ turns out to be more convenient. Based upon the analysis by Stone [32], one obtains (see also Appendix)

$$\Phi_{220}(\omega_i, \omega_j, \omega) = \frac{\sqrt{5}}{(4\pi)^{3/2}} P_2[\widehat{\boldsymbol{u}}(\omega_i) \cdot \widehat{\boldsymbol{u}}(\omega_j)], \tag{2.11a}$$

$$\Phi_{202}(\omega_i, \omega_j, \omega) = \frac{5}{(4\pi)^{3/2}} P_2[\widehat{\boldsymbol{u}}(\omega_i) \cdot \widehat{\boldsymbol{r}}_{ij}], \tag{2.11b}$$

$$\Phi_{022}(\omega_i, \omega_j, \omega) = \frac{5}{(4\pi)^{3/2}} P_2[\widehat{\boldsymbol{u}}(\omega_j) \cdot \widehat{\boldsymbol{r}}_{ij}], \tag{2.11c}$$

where $P_2(x) = \left(3x^2 - 1\right)/2$ is the second Legendre polynomial and $\widehat{\boldsymbol{u}}(\omega_i)$ and $\widehat{\boldsymbol{u}}(\omega_j)$ specify the orientation of mesogens i and j. Hence, with Eqs. (2.11a)–(2.11c) we can rewrite Eq. (2.10) as

$$\begin{aligned}\Psi(\widehat{\boldsymbol{r}}_{ij}, \omega_i, \omega_j) = {} & 5\varepsilon_1 P_2[\widehat{\boldsymbol{u}}(\omega_i) \cdot \widehat{\boldsymbol{u}}(\omega_j)] \\ & + 5\varepsilon_2 \{P_2[\widehat{\boldsymbol{u}}(\omega_i) \cdot \widehat{\boldsymbol{r}}_{ij}] \\ & + P_2[\widehat{\boldsymbol{u}}(\omega_j) \cdot \widehat{\boldsymbol{r}}_{ij}]\}.\end{aligned} \tag{2.12}$$

Hence, in GCEMC the interaction potential between a mesogenic pair follows from Eqs. (2.2), (2.9), and (2.12).

III. DENSITY-FUNCTIONAL THEORY

For the model introduced in Sec. II, we shall briefly sketch some key elements of DFT used in this work. Further details can be found in Refs. [33,34].

A. Modified mean-field grand potential functional

In DFT we are seeking coexisting equilibrium states for a given temperature T and chemical potential μ. In the absence of external fields (globally or meta) stable states are characterized by minima of the grand potential functional [see, for example, Eq. (1) of Ref. [35]]

$$\Omega[\rho(\boldsymbol{r},\omega)] = \mathcal{F}[\rho(\boldsymbol{r},\omega)] - \mu \int d\boldsymbol{r}\, d\omega\, \rho(\boldsymbol{r},\omega), \tag{3.1}$$

where $\mathcal{F}$ is the total free-energy functional and $\rho(\boldsymbol{r},\omega)$ is the orientation dependent local density. We follow our earlier work [33,34] in that we treat pair correlations in a so-called modified mean-field (MMF) fashion. At MMF level one approximates the orientation dependent pair correlation function by the Mayer f function $f(\boldsymbol{r}_{12},\omega_1,\omega_2) \equiv \exp[-\beta\varphi(\boldsymbol{r}_{12},\omega_1,\omega_2)] - 1$ ($\beta \equiv 1/k_{\mathrm{B}}T$, k_{B} Boltzmann's constant). This approximation becomes exact in the limit of vanishing density.

Here and following, we explicitly utilize the fact that our bulk system is homogeneous such that the orientation dependent local density can be decomposed according to $\rho(\boldsymbol{r},\omega) = \rho\alpha(\omega)$ where ρ is the mean number density. We expand the orientation distribution function $\alpha(\omega)$ in terms of Legendre polynomials $\{P_l\}$,

$$2\pi\alpha(\omega) \equiv \overline{\alpha}(x) = \frac{1}{2} + \sum_{l=1}^{\infty} \alpha_l P_l(x) \tag{3.2}$$

on account of the uniaxial symmetry of the N phase. In Eq. (3.2), $x \equiv \cos\vartheta$, and $\alpha_0 = \frac{1}{2}$. In the I phase, the set of order parameters $\{\alpha_l\}_{l\geqslant 1}$ vanishes identically; nonzero order parameters characterize the N phase.

Following the derivation detailed in Secs. III A and III B of Ref. [34] we can eventually express the grand potential as

$$\frac{\beta\Omega}{V} = \beta[f^{\mathrm{hs}} - \rho\mu] + \rho\int_{-1}^{1} dx\, \overline{\alpha}(x)\ln[2\overline{\alpha}(x)] + \rho^2 \sum_{l=0}^{\infty} \alpha_l^2 u_l, \tag{3.3}$$

where $f^{\mathrm{hs}} \equiv \mathcal{F}^{\mathrm{hs}}/V$ is the free-energy density of a hard-sphere reference fluid (including the ideal-gas contribution). For the configurational contribution to f^{hs} we adopt the well-known Carnahan-Starling expression [36]. In Eq. (3.3) and within the scope of the MMF approximation, the set of coupling coefficients $\{u_l\}_{l\geqslant 0}$

$$u_l = -\frac{(-1)^l}{\sqrt{\pi}(2l+1)^{3/2}} \int_{\sigma}^{\infty} dr_{12}\, r_{12}^2\, f_{ll0}(r_{12}). \tag{3.4}$$

They describe the contribution of intermolecular interactions to Ω [33,34]. In Eq. (3.4),

$$f_{ll0}(r_{12}) = 4\pi \int d\omega_1\, d\omega_2\, d\omega\, f(\boldsymbol{r}_{12},\omega_1,\omega_2) \times \Phi^*_{ll0}(\omega_1,\omega_2,\omega) \tag{3.5}$$

is a coefficient in the expansion of $f(\boldsymbol{r}_{12},\omega_1,\omega_2)$ [31].

The set of coefficients $\{f_{ll0}\}_{l\geqslant 0}$ in Eq. (3.5) may be evaluated employing a high-temperature expansion of the Mayer f function [see Eq. (3.5) of Ref. [33]]. Assuming $\beta\varphi_{\mathrm{anis}} \ll 1$, we expand the anisotropic part of the orientation dependent Mayer f function in a Taylor series retaining terms up to second order in $\beta\varphi_{\mathrm{anis}}$. Aside from the trivial coefficient f_{000} the first nontrivial contribution arises through f_{220}. This is because the anisotropic part of φ depends only on the rotational invariants Φ_{220}, Φ_{022}, and Φ_{202} given our current level of approximations (see Sec. II B) and because of the orthogonality of rotational invariants [see Eq. (3.12) of Ref. [33]]. Moreover, as has been argued by Groh and Dietrich [37], the contribution of terms proportional to α_l in Eq. (3.3) diminishes the larger l is. Hence, aside from the trivial term corresponding to α_0, which is always nonzero, we shall retain only the first nontrivial one corresponding to α_2 in Eq. (3.3). This necessitates the calculation of u_0 and u_2 for which f_{000} and f_{220} are required [see Eq. (3.4)].

Using the orthogonality of rotational invariants together with Eq. (3.31) of Ref. [33] and $\Phi_{000} = (4\pi)^{-3/2}$ we eventually arrive at

$$\frac{u_0}{8\pi} = -\mathcal{I}^{(0)} - \left(\frac{5}{2}\varepsilon_1^2 + \varepsilon_2^2\right)\mathcal{I}^{(2)}(\beta) \tag{3.6}$$

from Eq. (3.4) after tedious but relatively straightforward algebraic manipulations. In Eq. (3.6),

$$\mathcal{I}^{(n)}(\beta) \equiv \int_{\sigma}^{\infty} dr_{12}\, r_{12}^2\, [\beta\varphi_{\mathrm{att}}(r_{12})]^n \times \{\exp[-\beta\varphi_{\mathrm{iso}}(r_{12})] - \delta_{n0}\}, \tag{3.7}$$

where δ_{n0} is the Kronecker symbol. Likewise, we obtain

$$\frac{5u_2}{8\pi} = \varepsilon_1\mathcal{I}^{(1)}(\beta) - \left(\frac{5}{7}\varepsilon_1^2 + \frac{\sqrt{5}}{5}\varepsilon_2^2\right)\mathcal{I}^{(2)}(\beta) \tag{3.8}$$

after even more involved algebraic manipulations that we are not presenting in detail for the sake of conciseness. For more details, the interested reader is instead referred to our earlier publications [33,34]. Moreover, we note in passing that the remaining integrations in Eqs. (3.6) and (3.8) need to be carried out numerically. In practice, we employ the simple trapezoidal rule which is accurate enough if a one-dimensional mesh with a spacing of $10^{-2}\sigma$ between neighboring nodes is used.

B. Phase equilibrium

From the discussion in the preceding Sec. III A it is evident that Ω is a *function* of ρ and a *functional* of $\overline{\alpha}(x)$. Hence, thermodynamic equilibrium states are associated with minima of Ω with respect to ρ and $\overline{\alpha}(x)$. Therefore, we are seeking simultaneous solutions of the equations

$$\frac{\beta}{V}\left(\frac{\partial\Omega}{\partial\rho}\right) = 0, \tag{3.9}$$

$$\frac{\beta}{V}\frac{\delta\Omega}{\delta\overline{\alpha}(x)} = \lambda(T,\rho), \tag{3.10}$$

where λ is a Lagrangian multiplier introduced to make sure that $\overline{\alpha}(x)$ is properly normalized [34,35].

Consider now two phases labeled $'$ and $''$ coexisting at temperature T and pressure P. These phases may be characterized by their respective densities ρ' and ρ'' as well as by their orientational distributions $\overline{\alpha}'(x)$ and $\overline{\alpha}''(x)$. For the two phases to coexist, their densities and orientational

distributions have to satisfy

$$\frac{\Omega'}{V} = \frac{\Omega''}{V} = -P, \tag{3.11}$$

$$\frac{\beta}{V}\frac{\partial\,\Omega}{\partial\,\rho}\bigg|_{\rho',\overline{\alpha}'} = \frac{\beta}{V}\frac{\partial\,\Omega}{\partial\,\rho}\bigg|_{\rho'',\overline{\alpha}''}, \tag{3.12}$$

where P denotes pressure.

At this stage it is worthwhile to remind ourselves of the head-tail symmetry of the mesogens (see Sec. II B). Consequently, the orientation distribution function $\overline{\alpha}(x)$ must also be invariant under the transformation $\vartheta \to \vartheta' = \vartheta + \pi$ which implies that $\overline{\alpha}(x)$ must be an even function of x. This, in turn, suggests that $\alpha_l = 0$ if l is odd. We obtain the parameters $\{\alpha_l\}$ from

$$\alpha_l = \frac{2l+1}{2}\int_{-1}^{1} dx\,\overline{\alpha}(x)P_l(x). \tag{3.13}$$

Hence, the leading nontrivial term in the expansion (3.2) is the one for $l = 2$. Equation (3.13) is an immediate consequence of the orthogonality of the Legendre polynomials [see, for example, Eq. (A.9b) of Ref. [31]] and follows directly from Eq. (3.2).

Equation (3.11) may be rearranged such that for any given T, coexisting phases can be associated with solutions of the equation

$$\begin{aligned} 0 = s_1(T,\rho',\rho'',\alpha_2'') \equiv{}& \beta[f^{\rm hs}(T,\rho') - \rho'\mu^{\rm hs}(T,\rho')] \\ &- \beta[f^{\rm hs}(T,\rho'') - \rho''\mu^{\rm hs}(T,\rho'')] \\ &- \frac{u_0}{4}(\rho'^2 - \rho''^2) + \rho''^2 u_2 \alpha_2''^2, \end{aligned} \tag{3.14}$$

where we assume throughout this work that phase $'$ is always isotropic such that $\alpha_2' = 0$. If phase $''$ is isotropic, too [which is the case for the coexistence between gas (G) and I phases], the last summand on the third line of Eq. (3.14) vanishes identically. In Eq. (3.14), $\mu^{\rm hs} \equiv \left(\partial f^{\rm hs}/\partial\rho\right)_{T,V}$ is the chemical potential of the hard-sphere reference fluid [see Eqs. (3.11) and (3.27) of Ref. [34]].

Employing now the explicit expression for the Lagrangian multiplier λ [see, for example, Sec. III.D of Ref. [34]], Eq. (3.13) allows us to derive from Eq. (3.10) a second equation

$$\begin{aligned} 0 = s_2(T,\rho',\rho'',\alpha_2'') \equiv{}& \beta[\mu^{\rm hs}(T,\rho') - \mu^{\rm hs}(T,\rho'')] \\ &+ \frac{u_0}{2}(\rho' - \rho'') + \rho'' u_2 \alpha_2''^2 + \ln\frac{1}{2}\int_{-1}^{1} dx\,\Psi(x) \end{aligned} \tag{3.15}$$

which we solve numerically for its zeros as well. In Eq. (3.15),

$$\Psi(x) \equiv \exp[-5\rho'' u_2 \alpha_2'' P_2(x)]. \tag{3.16}$$

Because we consider terms up to $l = 2$ in the expansion of $\overline{\alpha}(x)$ in Eq. (3.2), we have one additional equation that needs to be solved self-consistently for α_2. This equation follows directly from Eq. (3.13) and the expression for the Lagrangian multiplier λ introduced in Eq. (3.10) [see Eqs. (3.28)–(3.30) of Ref. [34]]. More specifically, we solve

$$0 = s_4(T,\rho'',\alpha_2'') \equiv \alpha_2'' - \frac{5}{2}\frac{\int_{-1}^{1} dx\,\Psi(x)P_2(x)}{\int_{-1}^{1} dx\,\Psi(x)}. \tag{3.17}$$

Together, Eqs. (3.14), (3.15), and (3.17) form a system of three coupled, multivariate polynomial equations that can be solved iteratively by the lower and upper (LU) triangular decomposition method (see Appendix of Ref. [34]).

IV. MONTE CARLO SIMULATIONS

In the previous section, the grand potential functional is minimized to determine the phase boundaries for our liquid-crystal model. This approach is based upon three key assumptions, namely,

(1) the MMF approximation for pair correlations;

(2) the validity of the high-temperature expansion of the anisotropic part of the Mayer f function;

(3) the truncation of the expansion of the orientation distribution function after the first nontrivial term.

All three approximations are *a priori* uncontrollable and their performance can only be judged by comparison with another approach free of these assumptions. In this regard, the MC method is ideal because it is essentially a first-principles method in the sense that beyond the assumption of pairwise additive interactions [see Eq. (2.1)] and ergodicity, no other assumptions are invoked.

A. Basic considerations

Similar to Sec. III, the key quantity that we seek to compute here is the grand potential whose exact differential is given by

$$d\Omega = \frac{1}{k_{\rm B}\beta^2}\mathcal{S}\,d\beta + N\,d\mu - P\,dV, \tag{4.1}$$

where $\mathcal{S}$ is entropy. Because we are dealing with a homogeneous bulk fluid at constant T and μ, Ω is a homogeneous function of degree one in V. Thus, invoking Euler's theorem [38], $\overline{\omega} \equiv \Omega/V = -P$ immediately follows.

Hence, computing P as a function of T and μ we can obtain solutions of Eq. (3.11) for a pair of phases $'$ and $''$. To obtain a molecular expression for P, the key quantity is the grand canonical partition function [39,40]

$$\Xi = \sum_N \frac{\exp(\beta\mu N)}{N!\Lambda^{5N}}\left(\frac{\mathcal{I}}{2m}\right)^N \int d\boldsymbol{R}\,d\boldsymbol{\Omega}\,\exp[-\beta U(\boldsymbol{R},\boldsymbol{\Omega})] \tag{4.2}$$

for linear molecules where U is given in Eq. (2.1). In Eq. (4.2), $d\boldsymbol{R}\,d\boldsymbol{\Omega}$ is shorthand notation for $d\boldsymbol{r}_1 d\boldsymbol{r}_2 \ldots d\boldsymbol{r}_N d\omega_1 d\omega_2 \ldots d\omega_N$. The additional factor of $1/2^N$ takes notice of the head-tail symmetry of our mesogens. In addition, $\mathcal{I}$ is the moment of inertia of a mesogen, m is its mass, and $\Lambda = \sqrt{\beta h^2/2\pi m}$ is the thermal de Broglie wavelength where h denotes Planck's constant. Using now straightforward thermodynamic reasoning (see, for example, Sec. 3.3 of [31]), it is easy to verify that

$$\Omega = -\beta^{-1}\ln\Xi(\mu,V,T). \tag{4.3}$$

Because of Eq. (4.2), we need to generate microstates $(\boldsymbol{R},\boldsymbol{\Omega})$ distributed in configuration space according to the probability (density) $\exp\{-\beta[U(\boldsymbol{R},\boldsymbol{\Omega}) - \mu N] - \ln N! - 5N\ln\Lambda(\beta)\}$. To achieve this and because the mesogens have an aspect ratio slightly larger than one we adopt a modified version of

the algorithm suggested by Adams for spherical molecules [29]. This algorithm, which allows one to numerically realize a Markov process, proceeds in a sequence of steps. In the first one, each of the N mesogens is considered sequentially. It is then decided with equal probability whether to rotate the actual particle or to displace its center of mass. Depending on the associated change in energy, the rotation or displacement attempt is accepted (or rejected).

Once all N mesogens have been considered, it is attempted to change their number. During this second step, it is first decided with equal probability whether to remove one of the existing mesogens from the system or to add a new one at a randomly chosen position and with a randomly chosen orientation. Again, an energy criterion is employed to decide if the attempt is accepted. A total number of N' attempts is made where N' is the actual number of mesogens present in the system during the first step. The $2N'$ attempts constitute a MC cycle.

B. Properties

To identify equilibrium phases in GCEMC, we need to compute $\overline{\omega} = -P$. At fixed T, this is expected to be a single-valued function of μ in the one-phase region of any thermodynamic phase. However, because we also have from Eq. (4.1)

$$\left(\frac{\partial\overline{\omega}}{\partial\mu}\right)_{\beta,V} = -\rho, \tag{4.4}$$

we expect plots of $\overline{\omega}$ versus μ along a subcritical isotherm to have different slopes for any pair of phases having different densities. If phases $'$ and $''$ coexist at some $\mu = \mu_x$, $\overline{\omega}'(\mu_x) = \overline{\omega}''(\mu_x)$ such that the slope of $\overline{\omega}$ changes discontinuously at μ_x.

This approach obviously requires P as its key ingredient which we obtain from Clausius' virial. It states that

$$\begin{aligned}\frac{\beta P}{\rho} &= 1 + \left\langle \frac{\beta}{N}\sum_{i=1}^{N} \boldsymbol{r}_i \cdot \boldsymbol{F}_i \right\rangle \\ &= 1 + 24\beta\varepsilon\left\langle \frac{1}{N}\sum_{i=1}^{N}\sum_{\substack{j=1\\ j\neq i}}^{N} \varphi_{\mathrm{rep}}(r_{ij}) + \frac{1}{2}\varphi_{\mathrm{att}}(r_{ij}) \right. \\ &\quad \left. \times [1 + \Psi(\widehat{\boldsymbol{r}}_{ij}, \omega_i, \omega_j)] \right\rangle,\end{aligned} \tag{4.5}$$

where $\boldsymbol{F}_i$ is the total force exerted on mesogen i, $\langle \ldots \rangle$ denotes a grand canonical ensemble average, and Eqs. (2.1)–(2.3), and (2.9) have also been invoked.

Whereas the density difference $\Delta\rho = |\rho' - \rho''|$ is a suitable order parameter for condensation and evaporation because $\Delta\rho > 0$, a different order parameter is required to distinguish between ordered (i.e., N) and disordered (i.e., I) phases because here $\Delta\rho \simeq 0$ and therefore the slopes of $\overline{\omega}'$ and $\overline{\omega}''$ are hard if not impossible to distinguish. To introduce a suitable order parameter to analyze the IN phase transition, it has therefore been suggested quite some time ago by Eppenga and Frenkel [17] to consider the alignment tensor

$$\mathbf{Q} = \left\langle \frac{1}{2N}\sum_{i=1}^{N} [3\widehat{\boldsymbol{u}}(\omega_i) \otimes \widehat{\boldsymbol{u}}(\omega_i) - \mathbf{1}] \right\rangle, \tag{4.6}$$

where $\mathbf{1}$ is the unit tensor and $\otimes$ represents the tensor product. Hence, $\mathbf{Q}$ can be represented by a 3×3 matrix that is real, symmetric, and traceless. The alignment tensor satisfies the eigenvalue equation

$$\mathbf{Q}\widehat{\boldsymbol{n}}_{\pm,0} = \lambda_{\pm,0}\widehat{\boldsymbol{n}}_{\pm,0}, \tag{4.7}$$

which we solve numerically using Jacobi's method [41] to obtain the three eigenvalues $\lambda_- < \lambda_0 < \lambda_+$. Following standard practice [17], we take the largest eigenvalue $\lambda_+ = \mathcal{P}_2 = 2\alpha_2/5$ as the nematic order parameter and the associated eigenvector $\widehat{\boldsymbol{n}}_+$ as the nematic director.

According to its definition, $\lambda_+ = 0$ in the G or I phase. However, this is only true in the thermodynamic limit. In any computer simulation, where one inevitably deals with systems of finite extent, a small residual nematic order persists. This is because the interaction potential favors the formation of small domains in which mesogens tend to align their longer axes in a more or less parallel fashion. If the thermodynamic state pertains to the G or I phase, the correlation length associated with these domains vanishes more or less on the same length scale as does the interaction potential. Therefore, if two domains are sufficiently far apart, their *local* directors may point in different and uncorrelated directions. In a finite system, therefore, the global nematic order averages out up to a residual value which is the smaller the larger the system is. This is because in a larger system, more *local* domains exist over which one has to average to obtain the *global* nematic order parameter.

In a computer simulation, such finite-size effects are usually unwanted. However, one can turn this ostensible disadvantage into an advantage within the scope of finite-size scaling theory. Consider, for example, the distributions $p(\lambda_{+,0})$ of the largest and of the middle eigenvalue of $\mathbf{Q}$ which may be analyzed in terms of their moments

$$\langle \lambda_{+,0}^n \rangle \equiv \int_0^1 d\lambda_{+,0}\, \lambda_{+,0}^n\, p(\lambda_{+,0}). \tag{4.8}$$

In the context of finite-size effects at phase transitions, suitably defined cumulants of moments of the order-parameter distribution are of particular interest [42–44]. They are defined as ratios of moments of the order-parameter distribution where

$$g_n^{+,0} \equiv \frac{\langle \lambda_{+,0}^n \rangle}{\langle \lambda_{+,0} \rangle^n} \tag{4.9}$$

is the cumulant of nth order. In many cases, g_4 has been considered (see, for example, Refs. [44,45]). However, it is clear from Eqs. (4.8) and (4.9) that the larger n is, the more probed are the "wings" of the order-parameter distribution. Unfortunately, as one moves into these wings the statistical accuracy of p diminishes so that higher-order cumulants are expected to be less accurate. To avoid this difficulty, it had been suggested by Weber *et al.* [46] to use the lowest-order cumulant for which $n = 2$ in Eq. (4.9).

Moreover, following again Weber *et al.* [46] one anticipates

$$\langle \lambda_{+,0}^n(\cdot, L) \rangle = L^{n\beta/\nu}\mathcal{X}_{+,0}(\cdot, L/\ell) \tag{4.10}$$

at a *continuous* phase transition where L is the linear dimension of the (cubic) system under consideration. In this expression, β is the order-parameter critical exponent (not to be confused with $\beta = 1/k_B T$ as it is used everywhere else in this paper), ν is the critical exponent associated with the divergence of the correlation length ℓ, $\cdot$ stands for the thermodynamic field driving the transition, and $\mathcal{X}$ represents the so-called scaling function. Because $\mathcal{X}$ depends only on the ratio L/ℓ, g_n for different L have to intersect in a unique, albeit model-dependent point at which $\ell \to \infty$ (critical point) [44,47].

If the phase transition is *discontinuous* in principle but rounded on account of the finite size of the system, cumulants for different system sizes do not necessarily intersect in single point because ℓ remains finite. In this case, pairs of curves for different L may intersect in different points such that deviations of these points from a unique intersection scale as L^{-d} where d is the system dimension as was shown by Vollmayer *et al.* [47] for the q-states Potts model and by Weber *et al.* for a lattice model of flexible polymers [46]. In addition, Vollmayer *et al.* demonstrated that the "distance" of a unique cumulant intersection from the point at which the phase transition would occur in the thermodynamic limit scales as L^{-2d} [see Eqs. (34) and (36) of Ref. [47]]. Hence, if the system is sufficiently large, it may seem that even at a discontinuous phase transition all cumulants intersect in a unique point which then for all practical purposes may be taken as the state point at which the phase transition would occur in the thermodynamic limit.

V. RESULTS

Before turning to a discussion of results obtained in this work, it should be emphasized that all quantities are given in the usual dimensionless (i.e., "reduced") units. For example, lengths are given in units of σ and energies are given in units of ε. Other quantities are expressed in units of combinations of these basic quantities. For instance, we shall express temperatures in units of ε/k_B and pressures in units of ε/σ^3.

To solve Eqs. (3.14), (3.15), and (3.17), we employ the iterative scheme detailed in Appendix A of Ref. [34]. However, because of the more complex form of integrals related to the orientation distribution function in this study, these integrals are calculated numerically using a simple trapezoidal rule. Notice also that because of the free-energy functional used in this work, solid phases cannot be accounted for. Hence, only coexistence between fluidic (G, I, or N) phases has been considered.

In the parallel MC simulations, we cut off interactions between mesogens whose centers of mass are separated by a distance $r_c \geqslant 3.0$; no correction is applied for neglected interactions beyond r_c. The interaction potential remains unshifted at r_c. In addition, we employ a combination of a link cell and a Verlet neighbor list to further speed up the simulations. The implementation of both lists is described in Sec. 5.3 of the book by Allen and Tildesley [48]. Two mesogens are considered neighbors if their centers of mass are separated by a distance $r_N \leqslant 3.5$. Based upon previous experience with this model [30], we consider systems comprising between $N \approx 500$ and 2000 mesogens. Our results are based upon simulations comprising 10^4 MC cycles for equilibration followed by 10^5 cycles during which ensemble averages are computed.

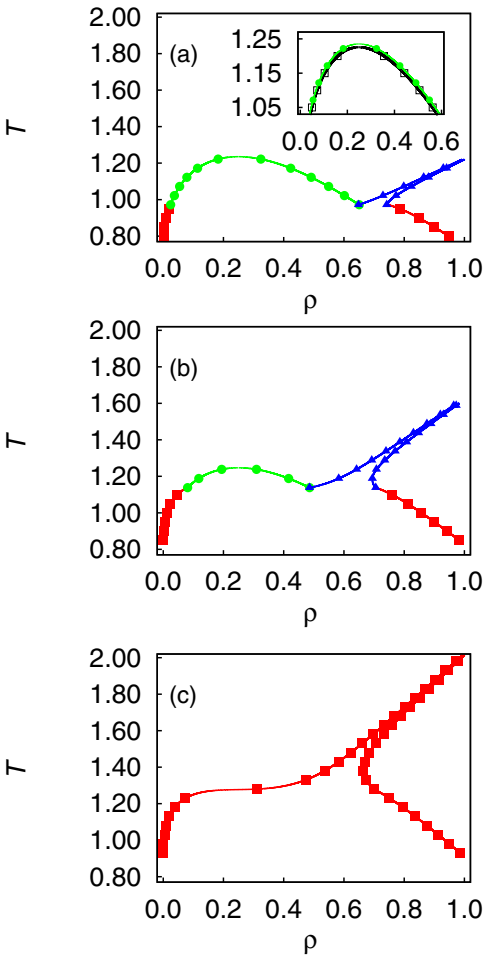

FIG. 1. (Color online) Phase diagrams in T-ρ representation showing coexistence between G and N (■, ——), G and I phases (●, ——), and I and N phases (▲, ——). In all parts of the figure $\varepsilon_2 = 0.00$; (a) $\varepsilon_1 = 0.04$, (b) $\varepsilon_1 = 0.06$, (c) $\varepsilon_1 = 0.08$. Inset in part (a) is an enhancement where data for $\varepsilon_1 = 0.0$ (□, ——) are also shown. Phase boundaries separate the G from the I phase for both data sets plotted in the inset.

A. Modified mean-field density-functional theory

We begin our presentation of results with phase diagrams generated within the framework of MMF DFT in Fig. 1. These phase diagrams have been generated by setting the anisotropy parameter $\varepsilon_2 = 0.00$ to study separately the impact of terms proportional to ε_1 and ε_2 in the anisotropy function Ψ [see Eq. (2.10)].

In the plot shown in Fig. 1(a) we see that for the smallest value $\varepsilon_1 = 0.04$, a G phase coexists with an N phase at sufficiently low T. As T increases above about 1.00, the N phase is eventually transformed into an I phase which is stable at lower densities up to $\rho \simeq 0.65$. At higher densities, IN phase coexistence is observed. Except for the lowest T at which IN phase coexistence is found, the densities of I and N phases are rather similar but never seem to become identically the same

within numerical resolution. In other words, there does not seem to be any critical point between I and N phases which is consistent with the phase diagram for the Gay-Berne model investigated by de Miguel *et al.* [27]. At $T_{\rm tr} \simeq 0.972$, a triple point exists in our model at which G, I, and N phases coexist.

In addition to the phase diagram of the liquid crystal, we also show the phase diagram of a simple Lennard-Jones fluid in the inset of Fig. 1(a). The Lennard-Jones fluid is a special case of the Hess-Su model realized by setting $\varepsilon_1 = \varepsilon_2 = 0.00$ in Eq. (2.11a). Notice again the absence of liquid-solid phase coexistence due to the form of the free-energy functional used here. By comparison between the Lennard-Jones and the Hess-Su phase diagrams, one notices from Fig. 1(a) that the orientation dependence of the mesogen-mesogen interaction is only of negligible importance as far as the phase boundaries between the G and I phases are concerned.

In particular, the critical temperatures $T_{\rm c} \simeq 1.226$ (Lennard-Jones) and $T_{\rm c} \simeq 1.235$ (Hess-Su) are nearly the same. Comparing $T_{\rm c}$ for the Lennard-Jones fluid from our MMF DFT with computer simulations of Potoff and Panagiotopoulos [49], who obtained a value of $T_{\rm c} \simeq 1.3120(7)$, reveals very good agreement between both approaches. However, the agreement is somewhat less satisfactory as far as the critical density is concerned. Here, our MMF DFT result $\rho_{\rm c} \simeq 0.249$ differs from the value $\rho_{\rm c} \simeq 0.316(1)$ reported by Potoff and Panagiotopoulos [49] by roughly 21%. Because the critical density is determined by packing effects, we suspect that a more satisfactory agreement would be obtainable if a more sophisticated form of the pair correlation function would have been used.

If ε_1 is increased to 0.06, the plot in Fig. 1(b) shows a topology of the phase diagram qualitatively similar to the one in Fig. 1(a). However, the triple point has shifted to a higher temperature $T_{\rm tr} \simeq 1.138$. One also notices by comparing plots in Figs. 1(a) and 1(b) that the density difference between I and N phases at $T_{\rm tr}$ increases with increasing coupling constant ε_1. At the same time, the critical temperature in Fig. 1(b) ($T_{\rm c} \simeq 1.247$) remains almost constant compared with the phase diagrams plotted in Fig. 1(a). This suggests that for sufficiently large ε_1, GI coexistence may be suppressed in favor of coexistence between a relatively dense isotropic phase and an N phase. This is indeed so as one can see from Fig. 1(c) for $\varepsilon_1 = 0.08$. Here, we see that the G-I near-critical regime visible in the plots in Figs. 1(a) and 1(b) has given way to a rather flat part of the coexistence curve centered more or less on $\rho \approx 0.30$.

The new feature in the phase diagram of our model liquid crystal as opposed to the "simple" Lennard-Jones potential is coexistence between relatively dense disordered and ordered phases. The degree of order exhibited by the latter can be quantitatively discussed in terms of the nematic order parameter $\mathcal{P}_2$. A plot of $\mathcal{P}_2$ as a function of T along the phase boundary of the N phase [see also Fig. 1(b)] shows that the order parameter decreases steadily with increasing T. Interestingly, $\mathcal{P}_2$ seems to level off at higher T and approaches a value of about 0.44. This "magic" number is also obtained in Mayer-Saupe theory as explained in the book by de Gennes and Prost [12]. As these latter authors point out, this limiting value is universal within the framework of Mayer-Saupe theory

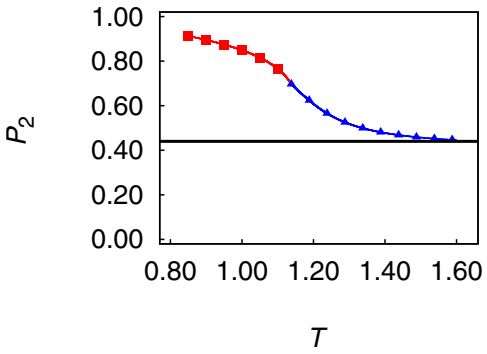

FIG. 2. (Color online) Plot of $\mathcal{P}_2$ as a function of temperature T for $\varepsilon_1 = 0.06$ [see Fig. 1(b)]. Data points refer to the higher-density phase boundaries between coexisting G-I (■, ——) and I-N phases (▲, ——). The horizontal line demarcates $\mathcal{P}_2 = 0.44$ (see text).

whereas it turns out to be temperature dependent in general within the framework of MMF DFT.

The approach of the Mayer-Saupe limit can be rationalized within MMF DFT. For sufficiently high T, $\mathcal{I}^{(2)}(\beta) \ll \mathcal{I}^{(1)}(\beta)$ such that Eq. (3.8) can be approximated by its leading term, that is,

$$\frac{5u_2}{8\pi} \approx \varepsilon_1 \mathcal{I}^{(1)}(\beta). \tag{5.1}$$

This expression can also be obtained by retaining in the expansion of the orientation dependent part of the Mayer f function only the leading term proportional to $\beta\varphi_{\rm anis}$ and computing f_{220} from Eq. (3.5). It is then clear that on account of the orthogonality of rotational invariants, the only contribution to f_{220} comes from the Mayer-Saupe term Φ_{220} [see Eq. (2.11a)] in the anisotropy function Ψ in Eq. (2.12). This explains why the Mayer-Saupe limit for $\mathcal{P}_2$ in Fig. 2 is reached for sufficiently high T. Deviations from this limiting value are to be expected for low T because then the above approximation is not valid and the full expression for u_2 in Eq. (3.8) has to be taken into account. Hence, because in the present analysis $\varepsilon_2 = 0$, a correction in proportion to ε_1^2 has to be considered in Eq. (3.8).

Next, we investigate the impact of ε_2 on the phase diagrams in Fig. 3. Comparing plots in Figs. 1 and 3, one notices that larger values of the coupling constant ε_2 are required in the latter case for the N phase to occur. This makes sense as one notices from Eq. (3.8) that ε_2 enters the MMF DFT quadratically in leading order. More specifically, the plot in Fig. 3(a) reveals that the N phase is completely absent such that only GI phase coexistence is observed. From the plots in the inset of Fig. 3(a) and the phase diagram of the Lennard-Jones fluid displayed in Fig. 1(a), the topological equivalence of both phase diagrams is evident. The only difference is that the critical temperature is a bit higher in Fig. 3(a).

At larger values of ε_2, plots in Figs. 3(b) and 3(c) indicate that coexistence between G, I, and N phases becomes possible such that from a topological perspective these phase diagrams are equivalent to the one shown in Fig. 1(b). Over the range of ε_2 for which our numerical technique is stable we fail to observe a phase diagram that would be topologically equivalent to the one depicted in Fig. 1(c).

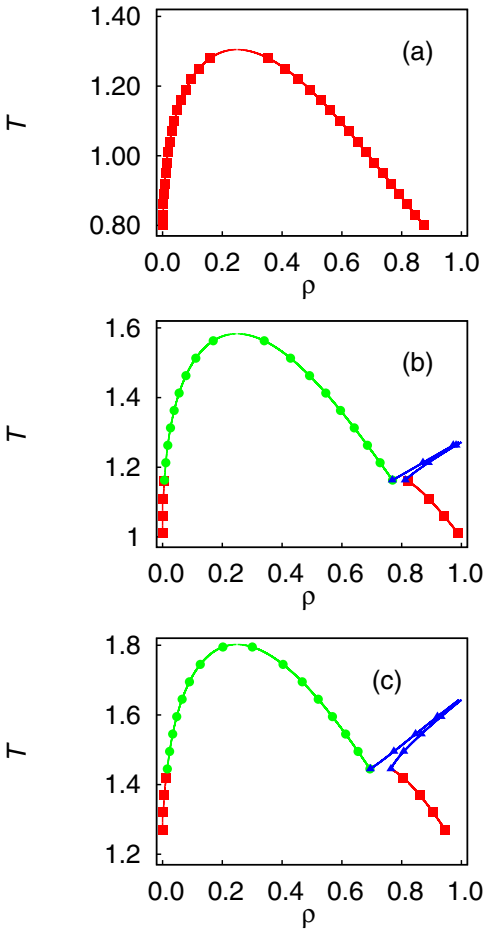

FIG. 3. (Color online) As Fig. 1, but for $\varepsilon_1 = 0.00$ and (a) $\varepsilon_2 = 0.12$, (b) $\varepsilon_2 = 0.29$, and (c) $\varepsilon_2 = 0.40$.

Moreover, unlike their counterparts in Fig. 1 the phase diagrams displayed in Fig. 3 show a pronounced impact of ε_2 on the GI critical point which appears to be elevated more the larger ε_2 is. Because of the dependence of the critical temperature on ε_2 it seems interesting to see to what an extent the law of corresponding states is obeyed by the present model. To that end, we focus on the "reduced" phase diagrams in Fig. 4.

In Fig. 4(a), we exhibit phase diagrams that are topologically equivalent for our choice of $\varepsilon_1 = 0.04$ unlike their counterparts presented in Fig. 3. In particular, we see from the plots in Fig. 4(a) that coexistence is obtained between all three phases accounted for by our model. If one renormalizes these phase diagrams to the respective GI critical-point location one sees from Fig. 4(b) that the curves shown in Fig. 4(a) can be superimposed in the GI near-critical regime, that is, in the temperature and density ranges $0.975 \lesssim T/T_c \leqslant 1.000$ and $0.75 \lesssim \rho/\rho_c \lesssim 1.25$, respectively. In this so defined near-critical regime, the law of corresponding states is approximately satisfied. Very much the same holds for a related model of an amphiphilic fluid where, however, the topology of the phase diagram is completely different [34] (see also Sec. VI).

As one moves out of the near-critical regime, plots in Fig. 4(b) reveal that the law of corresponding states is less well observed. Physically, this makes sense because one anticipates

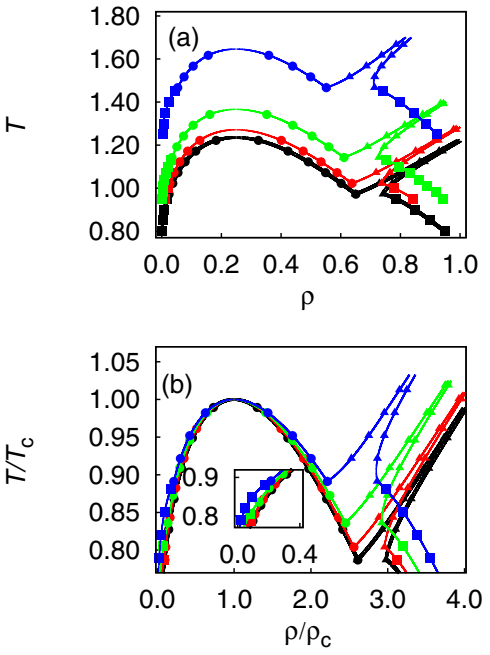

FIG. 4. (Color online) (a) As Fig. 1, but for $\varepsilon_1 = 0.04$ and (from bottom to top) $\varepsilon_2 = 0.00$, $\varepsilon_2 = 0.08$, $\varepsilon_2 = 0.16$, $\varepsilon_2 = 0.32$. Symbols refer to GN (■), GI (●), and IN (▲) phase coexistence. (b) As (a), but normalized to the respective critical temperature T_c and critical density ρ_c deduced from the plots in part (a) of the figure. Inset is an enlargement of a part of the G phase boundary.

details of the intermolecular interactions to become relevant as one moves away from the near-critical regime. The plots in Fig. 4(b) show that the part of the phase diagrams where the law of corresponding states is violated the most is the branch corresponding to IN phase coexistence. This observation is consistent with the fact that the IN phase transition is always first order and does not end in a critical point. Again, this feature is different for the related amphiphilic fluid where one observes a line of critical points separating isotropic from polar liquid phases very similar to the Curie line in ferroelectrics [34].

At this stage, it seems interesting to compare the MMF DFT phase diagram obtained in this work with the pseudo-phase diagrams presented earlier by Hess and Su [28] (see Fig. 5). We refer to the latter as "pseudo"-phase diagram because it has been determined such that for densities $\rho < 0.4$ "coexisting" states are actually loci of the spinodal, that is, thermodynamic states for which the isothermal compressibility becomes infinite. For densities $\rho > 0.4$, the phase boundary is determined through the condition $P(T,\rho) = 0$ which marks the limit of mechanical stability of the liquid phase.

However, it needs to be stressed that this determination of phase boundaries between G and I or N phases is an invalid procedure *in principle*. Not unexpectedly an inspection of Fig. 5 clearly reveals that the pseudo-phase diagram of Hess and Su [28] and the one determined here [which is based on the correct conditions for phase equilibria, see Eqs. (3.9) and (3.10)] are in complete disagreement.

In particular, one notices a discontinuity in the slope of the "phase boundary" of the I phase in the pseudo-phase diagram.

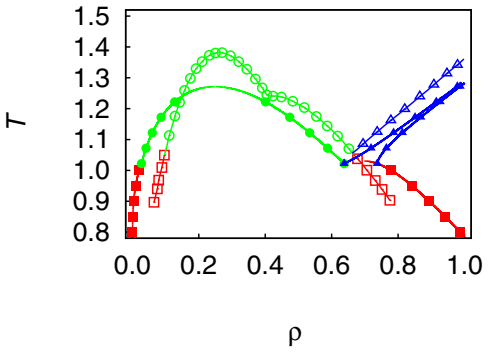

FIG. 5. (Color online) As Fig. 1, but for $\varepsilon_1 = 0.04$ and $\varepsilon_2 = -0.08$. Also shown is the pseudo-phase diagram (see text) presented in Fig. 6 of Ref. [28]. In the latter case, (□, ——), (○, ——), and (△, ——) refer to almost coexisting G and N, G and I, and I and N phases, respectively; (↓, - - -) demarcate the limiting density beyond which mechanical stability of liquid phases is used to determine the phase boundary (see text).

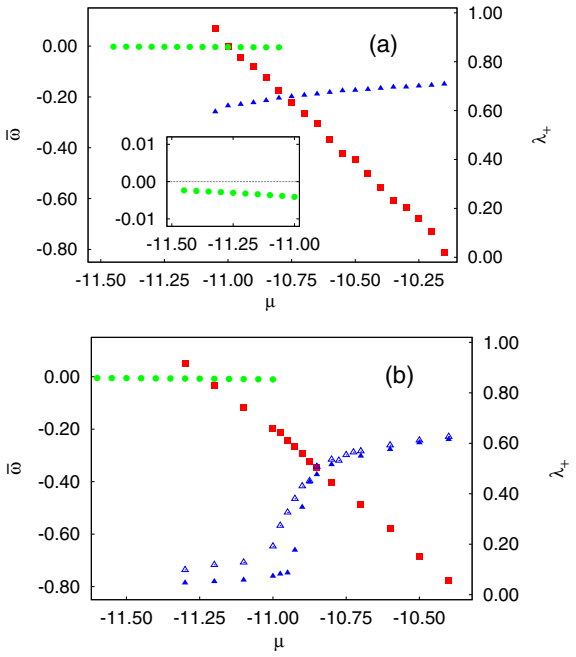

FIG. 6. (Color online) Plots of $\overline{\omega}$ (left ordinate) for G (●) and I and/or N phases (■) and λ_+ (△, ▲) (right ordinate) as functions of μ. (a) $T = 0.85$. The inset is an enhancement showing that G states are mechanically stable because of $\overline{\omega} < 0$. (b) $T = 0.90$ where $L = 10$ (△) and $L = 16$ (▲), respectively. Data for $\overline{\omega}$ are shown for $L = 16$ only. Results are obtained for $\varepsilon_1 = -\varepsilon_2/2 = 0.04$ (see Fig. 5).

This is an artifact that has to be attributed to the change in the criterion to determine the "phase boundary" at $\rho = 0.4$ (see above). Another peculiar and unrealistic feature of the pseudo-phase diagram is that the IN phase transition is predicted to occur without any change in density. The MMF DFT phase diagram, on the contrary, exhibits such a discontinuous density change along the IN phase boundary, albeit this change is always small and decreases even further as T increases.

The vanishing density difference between I and N phases predicted by Hess and Su [28] is, however, easy to explain. To estimate loci of the IN phase transition, Hess and Su employ a Landau expansion of the alignment free energy in terms of the nematic order parameter. In this phenomenological approach, one usually assumes the leading term to change sign at the onset of the IN phase transition. The constant of proportionality A governing this leading term is usually assumed to exhibit a linear dependence on the thermodynamic field driving the transition (i.e., T or P). Hence, within Landau theory the vanishing of A determines the value of the thermodynamic field at the onset of the IN phase transition. In the Landau expansion of Hess and Su, A is independent of ρ such that coexisting I and N phases cannot be discriminated with respect to ρ.

B. Grand canonical ensemble Monte Carlo

We now compare the predictions of the MMF DFT with GCEMC data. A careful selection of thermodynamic states is advisable based upon the following criteria:

(i) Selected isotherms should be removed sufficiently from the GI critical point to avoid the simulation to be hampered by critical slowing down.

(ii) Selected temperatures should be sufficiently high such that the density of the N phase at coexistence with either a G or an I phase is not too high ($\rho \lesssim 0.9$) and therefore the acceptance ratio for creation and deletion attempts remains significantly above 10^{-4}.

Based upon these selection criteria, we chose three isotherms at temperatures $T = 0.85$, 0.90, and 1.00 where for the latter Greschek and Schoen [30] already analyzed the IN phase transition in detail.

From the plots in Fig. 6(a) one sees that $\overline{\omega}$ consists of two branches characterized by markedly different slope. According to Eq. (4.4), the one of smaller slope corresponds to a G phase whereas the one exhibiting a larger slope is indicative of an I or N phase. One also sees that over a certain range of chemical potentials, $\overline{\omega}$ is a double-valued "function" of μ. The existence of this regime signals that on account of the small and finite size of the simulation cell, long-lived metastable states exist besides the thermodynamically stable states at the same μ. Obviously, for a given μ in the range where $\overline{\omega}$ is double valued, the larger value of $\overline{\omega}$ corresponds to the metastable state whereas the smaller one represents the thermodynamically stable state.

Both branches end at some μ where the respective metastable phase reaches its limit of stability and becomes unstable. These values of μ depend on system size. The two branches in the plot of $\overline{\omega}$ intersect at the chemical potential μ_x at which G and I or N phases coexist. Notice also that in both parts of Fig. 6, $\overline{\omega}$ for the metastable liquid phase becomes positive at a sufficiently low μ indicating that at this value the liquid phase turns out to be mechanically unstable.

At sufficiently high values of μ one also notices from Fig. 6(a) that the noise in the plot of $\overline{\omega}$ increases which reveals an increasing statistical error of our data because of the decreasing acceptance ratio for deletion and creation attempts at high densities (i.e., μ). This conclusion is corroborated by the corresponding plot in Fig. 6(b) which turns out to be much

smoother because the densities of the condensed I or N phase are lower at $T = 0.90$ as compared with $T = 0.85$.

In addition to the grand potential density we are also plotting the nematic order parameter λ_+ as a function of μ in Fig. 6. The plot in Fig. 6(a) shows that $0.60 \lesssim \lambda_+ \lesssim 0.70$ is relatively large throughout the regime in which the N phase is thermodynamically stable but decreases slightly with decreasing μ. Hence, the isotherm $T = 0.85$ is below $T_{\rm tr}$ as a comparison with Fig. 5 suggests.

By contrast, the corresponding plots in Fig. 6(b) suggest that at the slightly higher $T = 0.90$ an intermittent I phase exists. This is inferred from the strong decrease of λ_+ over a narrow range of chemical potentials as μ decreases. As μ is lowered, the condensed liquidlike phase loses its nematic order before the newly formed I phase reaches its phase boundary at which it coexists with the G phase. Hence, these results are consistent with the MMF DFT phase diagram presented in Fig. 5 if one assumes the isotherm $T = 0.90$ to be slightly above $T_{\rm tr}$.

One also notices from Fig. 6(b) that there is a distinct system size dependence visible in the plots of λ_+. Whereas both data sets agree nicely in the N phase, the plot of λ_+ for $L = 10$ exceeds its counterpart for $L = 16$ significantly in the I phase. In addition, one sees from Fig. 6(b) that in the vicinity of the transition from the N to the I phase the variation of λ_+ with μ for $L = 10$ is significantly more rounded than the corresponding curve for $L = 16$. The origin of the apparent system-size effect has already been explained in Sec. IV B.

To locate the IN phase transition despite the system-size dependent rounding of plots of λ_+, an analysis of the second-order cumulants defined in Eq. (4.9) is particularly useful. Plots of $g_2^{+,0}$ [see Sec. IV B and Eq. (4.9)] in Fig. 7 illustrate their characteristic variation in the vicinity of the IN phase transition. As demonstrated elsewhere [30], one expects $g_2^0 \propto N$ in the isotropic phase and sufficiently far away from the phase transition whereas g_2^+ should be system-size independent in this regime. Plots in Figs. 7(a) and 7(b) confirm this expectation (for a more detailed analysis of the scaling behavior of second-order cumulants, see Ref. [30]). As one increases μ, g_2^0 decreases monotonically irrespective of L. However, as the plots in Fig. 7(a) indicate, the magnitude of the slope of g_2^0 is the larger the larger L is in the vicinity of the IN phase transition such that all curves plotted in Fig. 7(a) intersect in a unique point at $\mu_{\rm x}^{\rm IN} \simeq -10.89$ demarcating the IN phase transition at $T = 0.90$. Hence, rounding in the vicinity of the IN phase transition diminishes with increasing L as expected.

The same unique intersection is found in plots of g_2^+ in Fig. 7(b). However, this quantity is more difficult to analyze because it passes through a maximum immediately before declining rapidly. The maximum turns out to be the more pronounced the larger the size of the system is. Characteristic features of both g_2^0 and g_2^+ are in qualitative agreement with observations made in Ref. [30] where, however, the thermodynamic field driving the transition is P rather than μ and a broader range of system sizes has been considered.

Comparing now plots in Fig. 7 with the one in Fig. 6(b), we realize that at $\mu_{\rm x}^{\rm IN}$ the plot of $\overline{\omega}$ does not exhibit a clear change in slope. Thus, according to Eq. (4.4) this implies that the IN phase transition is accompanied at best by a very minute

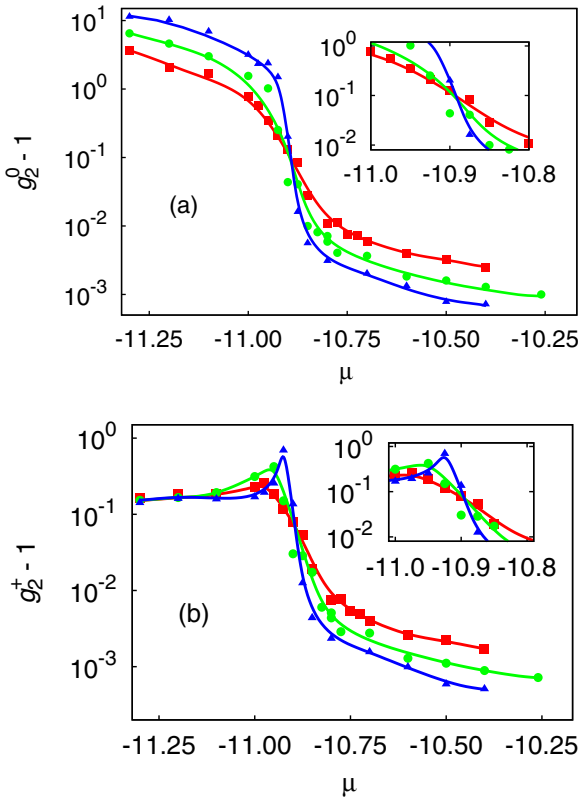

FIG. 7. (Color online) Semilogarithmic plots of g_2^0 (a) and g_2^+ (b) as functions chemical potential μ for $L = 10$ (■), $L = 13$ (●), and $L = 16$ (▲), and $T = 0.90$. Solid lines are intended to guide the eye.

change in density that is impossible to resolve on the basis of plots as in Fig. 6(b) [see also Eq. (4.4)].

That this is, in fact, so is shown in Fig. 8 where a plot of ρ versus μ at $T = 0.90$ does not exhibit any discontinuous change across the IN phase transition but appears to be rounded and continuous instead. However, two distinct branches of almost equal slope can be seen in the plot in Fig. 8. The apparent linear dependence of ρ on μ can be understood

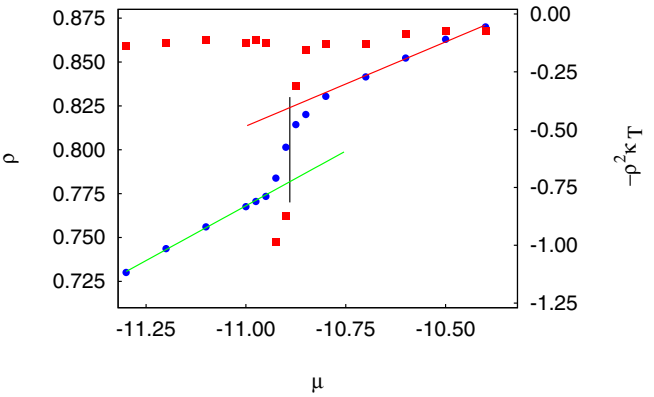

FIG. 8. (Color online) Plots of ρ (●) and of $-\rho^2\kappa_{\rm T}$ (■) as functions of chemical potential μ for $T = 0.90$. The vertical line (—) corresponds to $\mu_{\rm x}^{\rm IN} \simeq -10.89$ (see Fig. 7) whereas the red and green lines are linear fits to data points in the one-phase region of the I and N phases, respectively (see text).

if one considers the isothermal compressibility κ_T. To that end, one notices from elementary thermodynamic reasoning that

$$\left(\frac{\partial\rho}{\partial\mu}\right)_{T,V} = -\rho^2\kappa_T = -\frac{\beta}{V}(\langle N^2\rangle - \langle N\rangle^2) \qquad (5.2)$$

such that a linear dependence of ρ on μ implies that the right side of Eq. (5.2) is constant. Because β and V are maintained and because $\langle N^2\rangle - \langle N\rangle^2$ is a measure of density fluctuations in the grand canonical ensemble, these must be very similar in the I and N phases. Indeed, our data confirm this expectation for states sufficiently deep in the I and in the N phase as one can see from the plot in Fig. 8. One also notices from the plot in Fig. 8 that apparently density fluctuations increase markedly but only in the immediate vicinity of the IN phase transition as signaled by the sharp decline of $-\rho^2\kappa_T$ with increasing μ near μ_x^{IN}. Assuming that in the thermodynamic limit this linear variation of ρ with μ on the isotropic and on the nematic branch holds up to $\mu = \mu_x^{IN}$ we estimate a density difference of the I phase at coexistence with the G phase and at coexistence with the N phase of about $\Delta\rho \simeq 0.071$ from the plot in Fig. 8. This is the typical order of magnitude one anticipates from plots in Fig. 5 for states just above T_{tr}. Increasing the temperature to $T = 1.00$, $\Delta\rho \simeq 0.189$ between the I phase at the GI relative to the IN phase coexistence indicating that the width of the one-phase region of the I phase widens considerably as T increases. Again, this observation is in very good agreement with the MMF DFT phase diagram plotted in Fig. 5.

VI. DISCUSSION AND CONCLUSIONS

In this work, we investigate the phase behavior of a model liquid crystal by means of MMF DFT and GCEMC simulations. The interaction potential between a pair of mesogens consists of an isotropic Lennard-Jones core and a superimposed orientation dependent attractive contribution decaying as r^{-6} where r is the center-of-mass distance between a pair of mesogens. Hence, the interaction potential is short range corresponding to dispersion interactions.

The orientation dependent attractive term is derived by expanding it in terms of rotational invariants as a complete orthogonal set of basis functions. In addition, symmetry properties of the mesogens are exploited. In this work, we retain only the first three rotational invariants in our expansion which guarantees that aside from the G and the I phases, an N phase may also form. The final form of the orientation dependent contribution to the overall interaction potentials agrees with the one derived earlier by Hess and Su [28] who used an expansion in terms of irreducible Cartesian tensors instead of the (equivalent) expansion in rotational invariants used here.

The MMF DFT approach suggests two topologically different types of phase diagrams depending on the magnitude of the coupling constants of the orientation dependent terms in the interaction potential. In the first of these and for intermediate values of the coupling constants we have coexisting G and N phases at low temperatures. At higher T, we find separately coexistence between G and I and between I and N phases. This topology of the phase diagram seems generic.

We arrive at this conclusion by comparison with the bulk phase diagrams presented by Jungblut *et al.* [19]. Because in this latter work the interactions between all constituents are infinitely repulsive and of vanishing range, the IN phase transition is completely entropy driven. By contrast, it is a combination of entropic and energetic features that drive the IN phase transition in the present model. To compare with the work of Jungblut *et al.,* one needs to realize that the fugacity of the hard spheres in their model system plays the role of an inverse temperature in the present one such that the phase diagrams presented in the insets of Figs. 3 and 4 of Jungblut *et al.* appear to be turned upside down with respect to the ones shown here. Because the form of the potential used in their free-volume theory is the same as that employed in the corresponding MC simulations, Jungblut *et al.* [19] can also comment on the performance of the former. Perhaps not surprisingly they observe that the free-volume theory works well far away from the gas-liquid critical point but breaks down quantitatively in its vicinity.

As far as the density difference at the IN phase transition in the present model is concerned, this turns out to be very small and becomes almost negligible at temperatures only slightly above that of the triple point. Nevertheless, phase boundaries between I and N phases never seem to merge. In other words, a critical point between I and N phases does not seem to exist as expected. At higher coupling constants, the coexistence between G and I phases is suppressed entirely.

These general features of the phase behavior of the current model are distinctly different for a related model of an amphiphilic fluid recently studied by us [33,34]. Because of the polar nature of the amphiphiles an ordered polar (P) phase forms similar to the N phase in the present model. However, the phase behavior of the amphiphilic model is richer. For example, the P phase may coexist with an I phase or be separated from it along a line of critical points. Depending on details of the interaction potential, this critical line may either terminate in a critical end point or in a tricritical point.

To test the predictions of the MMF DFT, we employ GCEMC simulations. We focus on the topologically richest phase diagram and consider three isotherms. At the lowest T, we observe coexistence between a very dilute G and an N phase. At somewhat higher T, the G coexists with an I phase which undergoes a transition to an N phase only at even higher μ. The one-phase region of the I phase is narrow indicating that these first two isotherms are framing a triple point at which G, I, and N phases coexist. With increasing T, the one-phase region of the I phase widens considerably. All these features are consistent with the MMF DFT calculations.

It is particularly noteworthy that in this model the transition between I and N phases in GCEMC is severely rounded on account of the finite-system size. The transition is therefore not accompanied by a distinct discontinuous change in density. Instead, one observes only a continuous change in density as one goes from the I to the N phase.

These findings are again supported by the MMF DFT approach and also by a recent earlier computer simulation study by one of us [30]. In this earlier work, as in this one,

it turns out that second-order cumulants intersect in a unique point as one would expect if the IN phase transition were truly continuous. However, all other features such as the scaling of the maximum of the isobaric heat capacity, the variation of the order-parameter distribution across the transition, and a molecular-scale correlation length of orientational correlations pointed to the IN phase transition as a discontinuous rather than a continuous phase transition. This conclusion is now supported on the basis of the present more detailed MMF DFT calculations and the more extensive GCEMC simulations of this work.

It is perhaps also worth stressing that a difference between MMF DFT and GCEMC consists of the way in which short-range repulsive interactions are treated. In GCEMC, these are solely accounted for by $\varphi_{\rm rep}$ [see Eq. (2.3)] wheras in MMF DFT a "hard" repulsive core is used at $r_{ij} = \sigma$. To replace this "hard" core by a more realistic "soft" one is possible in principle by invoking perturbation approaches discussed in Chap. 5.3 of the book by Hansen and McDonald [50]. In essence, one replaces the hard-sphere diameter by an "effective" one that depends on the thermodynamic state under consideration. Whereas this might improve the *quantitative* agreement between MMF DFT and GCEMC, no attempts have been made here along these lines as we were more interested in *qualitative* generic features of the phase behavior of our liquid crystal.

As a next step of this study, it would be interesting to investigate the possible existence of smectic phases within the framework of the Hess-Su model. Work along these lines is currently under way.

ACKNOWLEDGMENT

We acknowledge financial support from the International Graduate Research Training Group 1524 "Self-assembled soft matter nanostructures at interfaces" and through Grant No. Scho 525-9.

APPENDIX: DERIVATION OF EQ. (2.11a)

In this Appendix, we rationalize Eq. (2.12). Our point of departure is the expression

$$\begin{aligned}\Phi_{220}(\omega_i,\omega_j,\omega) = \frac{1}{\sqrt{5}}\frac{1}{\sqrt{4\pi}}[&\mathcal{Y}_{22}(\omega_i)\mathcal{Y}_{2\underline{2}}(\omega_j)\\ &-\mathcal{Y}_{21}(\omega_i)\mathcal{Y}_{2\underline{1}}(\omega_j)+\mathcal{Y}_{20}(\omega_i)\mathcal{Y}_{20}(\omega_j)\\ &-\mathcal{Y}_{2\underline{1}}(\omega_i)\mathcal{Y}_{21}(\omega_j)+\mathcal{Y}_{2\underline{2}}(\omega_i)\mathcal{Y}_{22}(\omega_j)],\end{aligned} \tag{A1}$$

which follows directly from Eq. (2.5) where the prefactor $1/\sqrt{5}$ and the signs of individual terms are caused by the relevant Clebsch-Gordan coefficients. The second prefactor arises because $\mathcal{Y}_{00}(\omega) = 1/\sqrt{4\pi}$. We follow standard notation [31] in that the underscore of certain subscripts in Eq. (A1) indicates the negative value of the respective integer $m \geqslant 0$. Using

$$\mathcal{Y}_{l\underline{m}}(\omega) = (-1)^m \mathcal{Y}^*_{lm}(\omega), \tag{A2}$$

Eq. (A1) can then be rewritten as

$$\begin{aligned}\Phi_{220}(\omega_i,\omega_j,\omega) = \frac{1}{\sqrt{5}}\frac{1}{\sqrt{4\pi}}[&\mathcal{Y}_{22}(\omega_i)\mathcal{Y}^*_{22}(\omega_j)\\ &+\mathcal{Y}_{21}(\omega_i)\mathcal{Y}^*_{21}(\omega_j)+\mathcal{Y}_{20}(\omega_i)\mathcal{Y}_{20}(\omega_j)\\ &+\mathcal{Y}^*_{21}(\omega_i)\mathcal{Y}_{21}(\omega_j)+\mathcal{Y}^*_{22}(\omega_i)\mathcal{Y}_{22}(\omega_j)].\end{aligned} \tag{A3}$$

Let now

$$\widehat{\boldsymbol{u}}(\omega_i) = \begin{pmatrix}\sin\vartheta_i\cos\phi_i\\ \sin\vartheta_i\sin\phi_i\\ \cos\vartheta_i\end{pmatrix} = \begin{pmatrix}u_{xi}\\ u_{yi}\\ u_{zi}\end{pmatrix} \tag{A4}$$

such that [see Eq. (A.62) of Ref. [31]]

$$\begin{aligned}\mathcal{Y}_{20}(\omega_i)\mathcal{Y}_{20}(\omega_j) = \frac{5}{4\pi}\frac{1}{4}\big(&u^2_{xi}u^2_{xj}+u^2_{xi}u^2_{yj}-2u^2_{xi}u^2_{zj}\\ &+u^2_{yi}u^2_{xj}+u^2_{yi}u^2_{yj}-2u^2_{yi}u^2_{zj}\\ &-2u^2_{zi}u^2_{xj}-2u^2_{zi}u^2_{yj}+4u^2_{zi}u^2_{zj}\big),\end{aligned} \tag{A5}$$

where the normalization of $\widehat{\boldsymbol{u}}_i$ has also been utilized. Next, employing the identity

$$e^{i\phi_i}e^{-i\phi_j}+e^{-i\phi_i}e^{i\phi_j} = 2(\cos\phi_i\cos\phi_j+\sin\phi_i\sin\phi_j), \tag{A6}$$

one obtains

$$\begin{aligned}&\mathcal{Y}_{21}(\omega_i)\mathcal{Y}^*_{21}(\omega_j)+\mathcal{Y}^*_{21}(\omega_i)\mathcal{Y}_{21}(\omega_j)\\ &\quad= 3\frac{5}{4\pi}(u_{xi}u_{xj}u_{zi}u_{zj}+u_{yi}u_{yj}u_{zi}u_{zj}).\end{aligned} \tag{A7}$$

Finally, after some straightforward algebra, one finds

$$\begin{aligned}&\mathcal{Y}_{22}(\omega_i)\mathcal{Y}^*_{22}(\omega_j)+\mathcal{Y}^*_{22}(\omega_i)\mathcal{Y}_{22}(\omega_j)\\ &\quad= \frac{5}{4\pi}\frac{3}{4}\big[u^2_{xi}u^2_{xj}-u^2_{yi}u^2_{xj}-u^2_{xi}u^2_{yj}+u^2_{yi}u^2_{yj}\\ &\qquad+4u^2_{xi}u^1_{yj}u^2_{xj}u^2_{yj}\big]\end{aligned} \tag{A8}$$

which follows from the definition of $\mathcal{Y}_{22}$ [see Eq. (A.62) of Ref. [31]], Eq. (A4), and the identity

$$\begin{aligned}&e^{2i\phi_i}e^{-2i\phi_j}+e^{-2i\phi_i}e^{2i\phi_j}\\ &\quad= 2[\cos^2\phi_i\cos^2\phi_j-\sin^2\phi_i\sin^2\phi_j\\ &\qquad-\cos^2\phi_i\sin^2\phi_j+\sin^2\phi_i\sin^2\phi_j\\ &\qquad+4\cos\phi_i\sin\phi_i\cos\phi_j\sin\phi_j].\end{aligned} \tag{A9}$$

From Eqs. (A5), (A7), and (A8), one eventually obtains

$$\begin{aligned}&u^2_{xi}u^2_{xj}+u^2_{yi}u^2_{yj}+u^2_{zi}u^2_{zj}-\frac{1}{2}\big[\big(u^2_{yi}+u^2_{zi}\big)u^2_{xj}\\ &\qquad+\big(u^2_{xi}+u^2_{yi}\big)u^2_{zj}+\big(u^2_{xi}+u^2_{zi}\big)u^2_{yj}\big]\\ &\qquad+3[u_{xi}u_{zi}u_{xj}u_{zj}+u_{xi}u_{yi}u_{xj}u_{yj}+u_{yi}u_{zi}u_{yj}u_{zj}]\\ &\quad= P_2[\widehat{\boldsymbol{u}}(\omega_i)\cdot\widehat{\boldsymbol{u}}(\omega_i)]\end{aligned} \tag{A10}$$

which follows directly if one also utilizes the fact that both $\widehat{\boldsymbol{u}}(\omega_i)$ and $\widehat{\boldsymbol{u}}(\omega_j)$ are normalized to one. The above derivation goes through identically if one replaces either $\widehat{\boldsymbol{u}}(\omega_i)$ or $\widehat{\boldsymbol{u}}(\omega_j)$ by $\widehat{\boldsymbol{u}}(\omega)$ which is a unit vector specifying the orientation of $\widehat{\boldsymbol{r}}$. However, in both cases, the Clebsch-Gordan coefficients are all equal to one and therefore the prefactors in Eqs. (2.11b) and (2.11c) differ from the one in Eq. (2.11a) by a factor of $5/\sqrt{5}$.

[1] I. A. Shanks, Contemp. Phys. **23**, 65 (1982).
[2] R. A. M. Hikmet and H. Kempermann, Nature (London) **392**, 476 (1998).
[3] O. Guzmán, N. L. Abbott, and J. J. de Pablo, J. Chem. Phys. **122**, 184711 (2005).
[4] A. Hussain, A. S. Pina, and A. C. A. Roque, Biosens. Bioelectron. **25**, 1 (2009).
[5] S. V. Shiyanovskii, T. Schneider, I. I. Smalyukh, T. Ishikawa, G. D. Niehaus, K. J. Doane, C. J. Woolverton, and O. D. Lavrentovich, Phys. Rev. E **71**, 020702 (2005).
[6] F.-J. Carrión, G. Martínez-Nicolás, P. Iglesias, J. Sanes, and M.-D. Bermúdez, Int. J. Mol. Sci. **10**, 4102 (2010).
[7] D. Kang, J. E. Maclennan, N. A. Clark, A. A. Zakhidov, and R. H. Baughman, Phys. Rev. Lett. **86**, 4052 (2001).
[8] S. Juodzakis, V. Mizeikis, and H. Misawa, J. Appl. Phys. **106**, 051101 (2009).
[9] W. Pisula, M. Zorn, J. Y. Chang, K. Müllen, and R. Zentel, Macromol. Rapid Commun. **30**, 1179 (2009).
[10] S.-H. Yang and C.-S. Hsu, J. Polym. Sci., Part A: Polym. Chem. **47**, 2713 (2009).
[11] K. Larsson, Curr. Opin. Colloid Interface Sci. **14**, 16 (2009).
[12] P. G. de Gennes and J. Prost, *The Physics of Liquid Crystals* (Clarendon, Oxford, 1995).
[13] L. Onsager, Ann. N. Y. Acad. Sci. **51**, 627 (1949).
[14] W. Maier and A. Saupe, Z. Naturforsch. A **13**, 564 (1959).
[15] W. Maier and A. Saupe, Z. Naturforsch. A **14**, 882 (1959).
[16] W. Maier and A. Saupe, Z. Naturforsch. A **15**, 287 (1960).
[17] R. Eppenga and D. Frenkel, Mol. Phys. **52**, 1303 (1984).
[18] S. C. McGrother, D. C. Williamson, and G. Jackson, J. Chem. Phys. **104**, 6755 (1995).
[19] S. Jungblut, R. Tuinier, K. Binder, and T. Schilling, J. Chem. Phys. **127**, 244909 (2012).
[20] F. Oosawa and S. Asakura, J. Chem. Phys. **22**, 1255 (1954).
[21] A. Vrij, Pure Appl. Chem. **48**, 471 (1976).
[22] H. N. W. Lekkerkerker and A. Stroobants, Nuovo Cimento D **16**, 949 (1994).
[23] T. Kihara, Adv. Chem. Phys. **5**, 147 (1963).
[24] A. Cuetos, B. Martínez-Haya, S. Lago, and L. F. Rull, Phys. Rev. E **68**, 011704 (2003).
[25] J. G. Berne and B. J. Berne, J. Chem. Phys. **74**, 3316 (1981).
[26] B. J. Berne and P. Pechukas, J. Chem. Phys. **56**, 4213 (1972).
[27] E. de Miguel, L. F. Rull, M. K. Chalam, and K. E. Gubbins, Mol. Phys. **74**, 405 (1991).
[28] S. Hess and B. Su, Z. Naturforsch. A **54**, 559 (1999).
[29] D. J. Adams, Mol. Phys. **29**, 307 (1975).
[30] M. Greschek and M. Schoen, Phys. Rev. E **83**, 011704 (2011).
[31] C. G. Gray and K. E. Gubbins, *Theory of Molecular Fluids*, Vol. 1 (Clarendon, Oxford, 1984).
[32] A. J. Stone, Mol. Phys. **36**, 241 (1978).
[33] S. Giura, B. G. Márkus, S. H. L. Klapp, and M. Schoen, Phys. Rev. E **87**, 012313 (2013).
[34] M. Schoen, S. Giura, and S. H. L. Klapp, Phys. Rev. E **89**, 012310 (2014).
[35] J. M. Tavares, M. M. Telo da Gama, P. I. C. Teixeira, J. J. Weis, and M. J. P. Nijmeijer, Phys. Rev. E **52**, 1915 (1995).
[36] N. F. Carnahan and K. E. Starling, J. Chem. Phys. **51**, 635 (1969).
[37] B. Groh and S. Dietrich, Phys. Rev. E **50**, 3814 (1994).
[38] M. Schoen and S. H. L. Klapp, *Nanoconfined Fluids: Soft Matter Between Two and Three Dimensions* (Wiley-VCH, Weinheim, 2007).
[39] D. A. McQuarrie, *Statistical Mechanics* (University Science Books, Sausalito, CA, 2000).
[40] T. Gruhn and M. Schoen, Phys. Rev. E **55**, 2861 (1997).
[41] W. T. Press, S. A. Teukolsky, W. T. Vetterling, and B. P. Flannery, *Numerical Recipes in FORTRAN 90* (Cambridge University Press, Cambridge, UK, 1996).
[42] K. Binder, Z. Phys. B: Condens. Matter **43**, 119 (1981).
[43] K. Binder, Phys. Rev. Lett. **47**, 693 (1981).
[44] D. P. Landau and K. Binder, *A Guide to Monte Carlo Simulations in Statistical Physics* (Cambridge University Press, Cambridge, UK, 2005).
[45] K. Binder and D. W. Heermann, *Monte Carlo Simulation in Statistical Physics* (Springer, Berlin, 1988).
[46] H. Weber, W. Paul, and K. Binder, Phys. Rev. E **59**, 2168 (1999).
[47] K. Vollmayer, J. D. Reger, M. Scheucher, and K. Binder, Z. Phys. B: Condens. Matter **91**, 113 (1993).
[48] M. Allen and D. Tildesley, *Computer Simulation of Liquids* (Oxford University Press, Oxford, UK, 1986).
[49] J. J. Potoff and A. Z. Panagiotopoulos, J. Chem. Phys. **109**, 10914 (1998).
[50] J.-P. Hansen and I. R. McDonald, *Theory of Simple Liquids* (Academic, London, 2006).